Supporting Information

Hybrid MOF-808-Tb nanospheres for highly sensitive and selective detection of acetone vapor and Fe^{3+} in aqueous solution

Jian Zhang,[a] Shing Bo Peh,[a] Jian Wang,[a] Yonghua Du,[b] Shibo Xi,[b] Jinqiao Dong,[a] Avishek Karmakar,[a] Yunpan Ying,[a] Yuxiang Wang,[a] and Dan Zhao*[a]

[a] Department of Chemical and Biomolecular Engineering, National University of Singapore, 4 Engineering Drive 4, 117585 Singapore
[b] Institute of Chemical and Engineering Sciences, A*STAR, Jurong Island, 627833 Singapore

E-mail: chezhao@nus.edu.sg

Table of Contents

Experiment Section

Materials

All the chemicals were obtained from commercial sources and used without further purification. The standard stock solutions of metal ions (10 mM) were prepared with ultrapure water from the respective metal nitrate. The ultrapure water was supplied by a water purification system, PU^+.

Microwave-assisted synthesis of MOF-808 nanospheres

Considering the green chemistry and energy conservation, MOF-808 nanospheres were synthesized by a microwave-assisted synthesis process in aqueous solution. In brief, $ZrOCl_2$ (0.38 g, 1.2 mmol) and H_3BTC (0.31 g, 1.8 mmol) were dissolved in water under sonication. The reaction solution was then transferred into a glass tube and sealed. The tube was placed into a microwave synthesizer (Anton Paar MW450) and heated to 95 °C within 2 min. After that, the whole system was held at that temperature for 4 h under stirring (800 rpm), and then cooled down to room temperature. The as-synthesized powder was collected by centrifugation at 8000 rpm, washed with fresh methanol (MeOH) for several times, and air-dried for further usage.

Post-synthetic modification process of MOF-808 nanospheres

The hybrid MOF-808-Tb nanospheres were synthesized by a solution-phase metalation process. Typically, the as-synthesized MOF-808 nanospheres (50 mg) were added to 20 mL of $Tb(NO_3)_3{\cdot}6H_2O$/ethanol solution (20 mg mL^{-1}). The mixture was sonicated for 20 min and

40 μL of triethylamine was added under stirring at room temperature. After that, the solution was heated at 80 °C for 4 h and cooled down to room temperature. Finally, the solid products were collected by centrifugation at 8000 rpm and washed by ethanol several times. To explore the suitable synthetic conditions, several comparison experiments were conducted. The MOF-808-TB-1h and MOF-808-Tb-6h were synthesized under the same conditions with varying heating times (1 h and 6 h, respectively). The MOF-808-Tb-6h has a higher Tb content but with lower crystallinity. Therefore, we can conclude that the abundant unsaturated coordination sites in the framework of MOF-808 can offer ample sites for Tb grafting, but too much Tb grafting will cause structural collapse.

Luminescent sensing experiments

All the luminescent chemical sensing tests were carried out on a PTI QuantaMaster 800 spectrofluorometer at room temperature using an excitation wavelength of 290 nm.

1. Solution-based chemical sensing test: MOF-808-Tb nanospheres (0.4 mg) were added to different solvents (2.0 mL) to obtain different suspensions and each suspension was treated by ultrasonication thoroughly before the tests. To further characterize the quenching behaviour, titration of MOF-808-Tb with acetone was performed with hexane as the inert solvent. As shown in **Fig. S7**, the intensities of fluorescence spectra decreased with the addition of acetone and hexane mixed solution ($V_{acetone}/V_{hexane}$ = 1:1000, 1 μL solution is about 0.6 ppb).

2. Acetone vapor fluorescent response test: MOF-808-Tb nanospheres (about 0.2 mg) were adhered to the walls of the cuvette, and 1 μL of acetone was then introduced to the

bottom of cuvette. The cuvette was covered promptly, and the fluorescence spectra were recorded one minute later. The reproducibility was confirmed by multiple testing cycles with the same sample. Between each experiment, the cuvette with sample was heated to 80 °C to remove the adsorbed acetone. The concentration of acetone vapor was estimated by assuming ideal gas behavior of the air within the cuvette, i.e. $c \approx (\frac{1\ \mu L \times \rho_{acetone}}{MW_{acetone}}) \div \left(\frac{PV_{cuvette}}{RT}\right)$ where ρ is the liquid density of acetone.

3. In typical quenching trials, the fluorescence spectra in aqueous solution was measured by the incremental addition of various metal ions (10^{-2} M, 0.2 mL) in the MOF-808-Tb suspension (2 mL, 0.2 mg/mL). The degree of quenching was defined as $(I_0\text{-}I)/I_0$ (where I_0 and I denote the intensities before and after metal ion addition, respectively). The interference studies were tested and described as follows: another cation solution (10^{-2} M, 0.2 mL) was added to the suspension (2 mL, 0.2 mg/mL) and the luminescence intensity was monitored, then Fe^{3+} ion solution (10^{-2} M, 0.2 mL) was added into the mixture and the emission spectrum was measured after several minutes. The reproducibility of MOF-808-Tb nanospheres was also studied under the same condition.

Characterization

Powder X-ray diffraction (PXRD) data of all the products were collected on a Rigaku MiniFlex 600 powder X-ray diffractometer with Cu K_α radiation (λ = 1.5418 Å). The as-synthesized MOF-808 nanospheres and MOF-808-Tb nanospheres were characterized by field-emission scanning electron microscopy (FESEM, JEOL, JSM-7610F) and transmission electron microscopy (TEM, JEOL, JEM-3010). N_2 sorption isotherms were measured on a Micromeritics ASAP 2020 at 77 K. The guest molecules in the frameworks of MOF-808 and MOF-808-Tb were exchanged with fresh methanol several times before activation under vacuum (120 °C for 10 h). The thermal gravimetric analyses (TGA) were performed by using Shimadzu DTG-60AH under an air flow at a rate of 10 °C min^{-1} from 50 °C to 800 °C. X-ray photoelectron spectra (XPS) were tested using a Kratos AXIS Ultra XPS system (Kratos Analytical Ltd) with a monochromatic Al K_α radiation source (1486.6 eV) at 15 kV. The solid-state UV-vis spectra were detected by a SHIMADZU UV-2450 spectrophotometer in the range of 400-800 nm using $BaSO_4$ as the standard. Fourier transform infrared (FTIR) spectra were obtained by a Bio-Rad FTS-3500 ARX FTIR spectrometer**.** The dynamic laser scattering (DLS) data were recorded by a NanoBrook Omni instrument. The elemental analysis of samples was detected by Inductive Coupled Plasma-Optical Emission Spectroscopy (ICP-OES, Perkin Elmer Optima 5300DV). The Tb L-edge X-ray absorption fine structure (XAFS) spectra were measured under transmission mode at the XAFCA beamline of Singapore Synchrotron Light Source (SSLS).

Stern–Volmer equation calculation

$$\frac{I_0}{I} = 1 + K_{SV}[Fe^{3+}]$$

where I_0 is the initial emission intensity of MOF-808-Tb prior to the addition of the quencher, I is the emission intensity at any given concentration $[Fe^{3+}]$ of the quencher and K_{SV} is the Stern-Volmer constant.

Morphologies, Physical and Chemical Properties

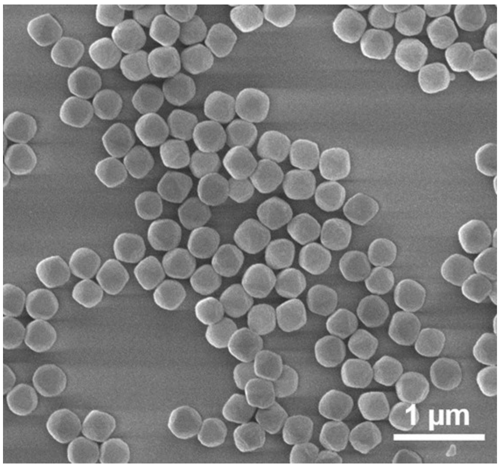

Fig. S1. The SEM image of MOF-808 nanospheres.

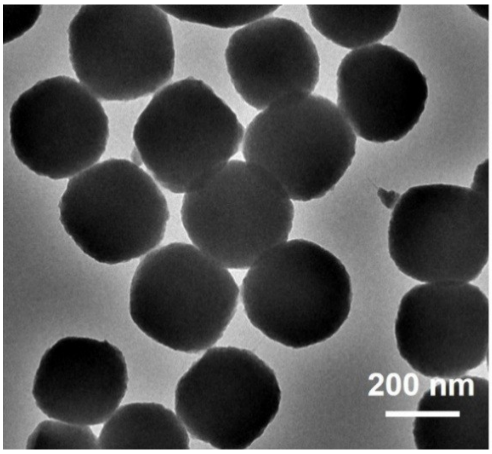

Fig. S2. The TEM image of MOF-808 nanospheres.

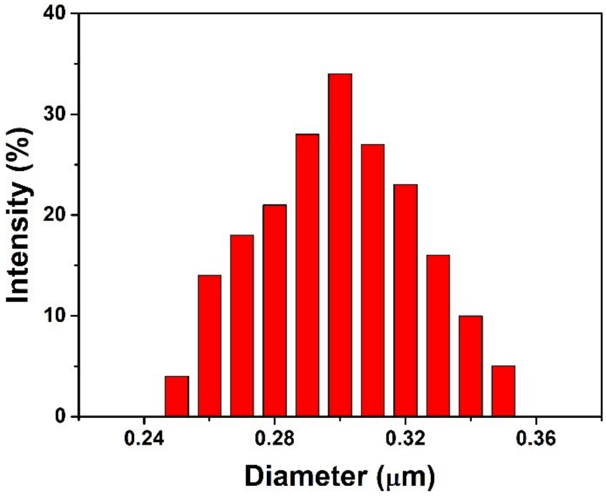

Fig. S3. Histogram of the particle size distribution of MOF-808-Tb nanospheres on the basis of dynamic light scattering results.

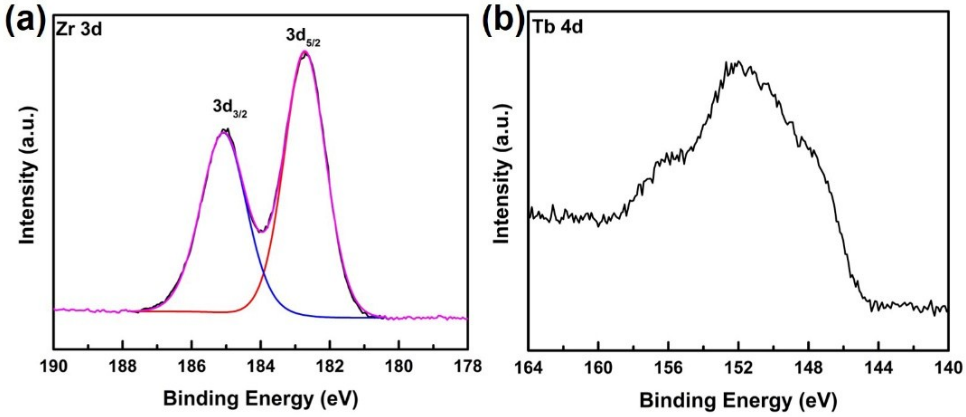

Fig. S4. Detailed XPS spectra of the Zr 3d and Tb 4d region in MOF-808-Tb.

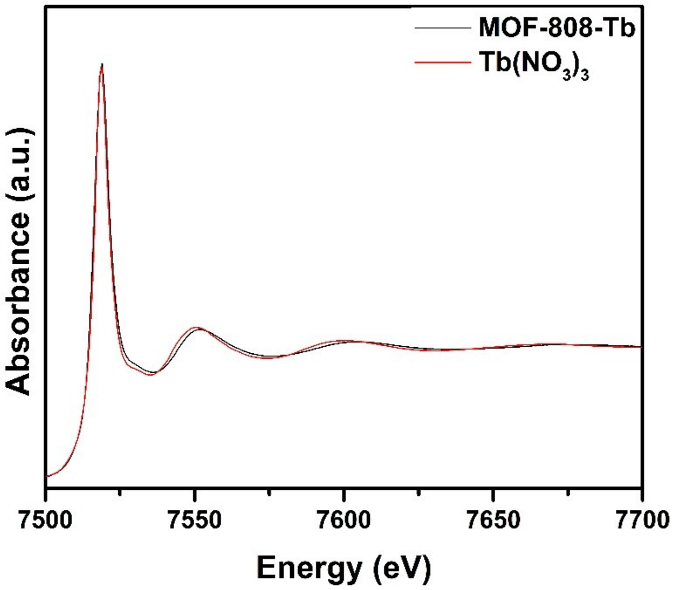

Fig. S5. Tb L-edge X-ray absorption near edge structure (XANES) data comparison between MOF-808-Tb and Tb(NO$_3$)$_3$.

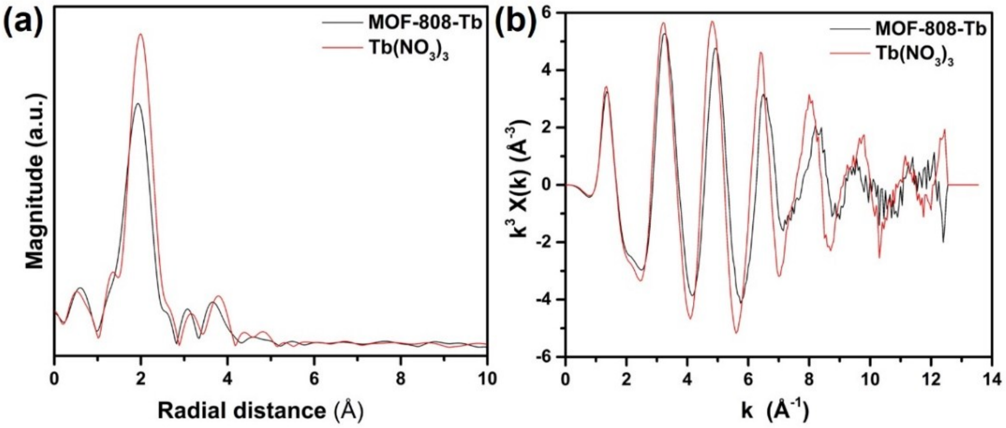

Fig. S6. (a) Fourier transformed EXAFS data of Tb L edge from MOF-808-Tb and Tb(NO$_3$)$_3$; (b) EXAFS *k*-space spectra (k^3-weighted) of MOF-808-Tb and Tb(NO$_3$)$_3$ from Tb L3.

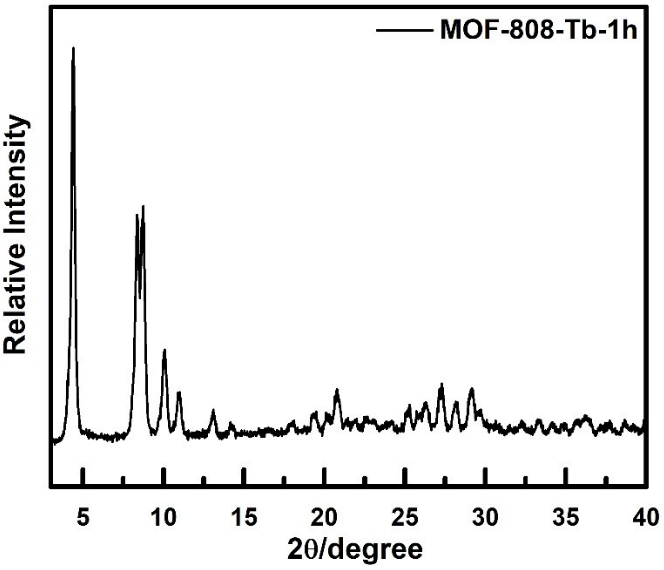

Fig. S7. The PXRD pattern of as-synthesized MOF-808-Tb-1h.

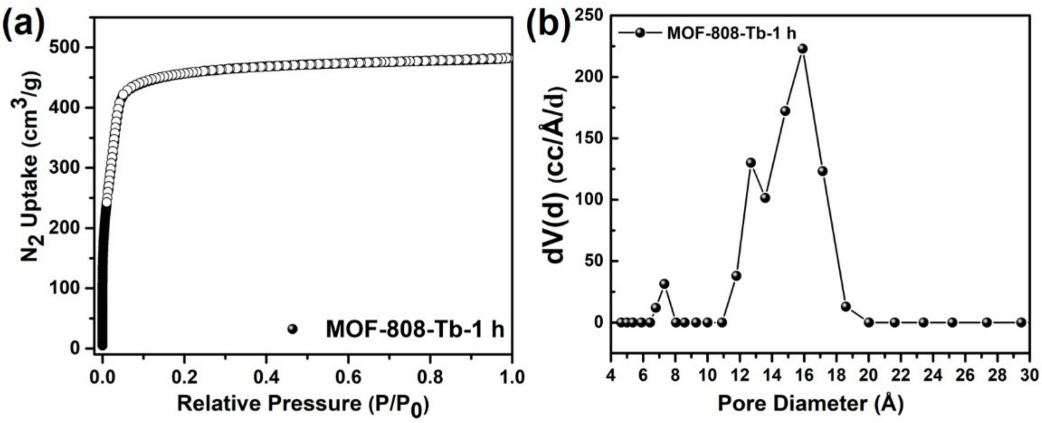

Fig. S8. (a) 77 K N_2 sorption isotherm and (b) pore size distribution of as-synthesized MOF-808-Tb-1h. Closed symbol, adsorption; open symbol, desorption.

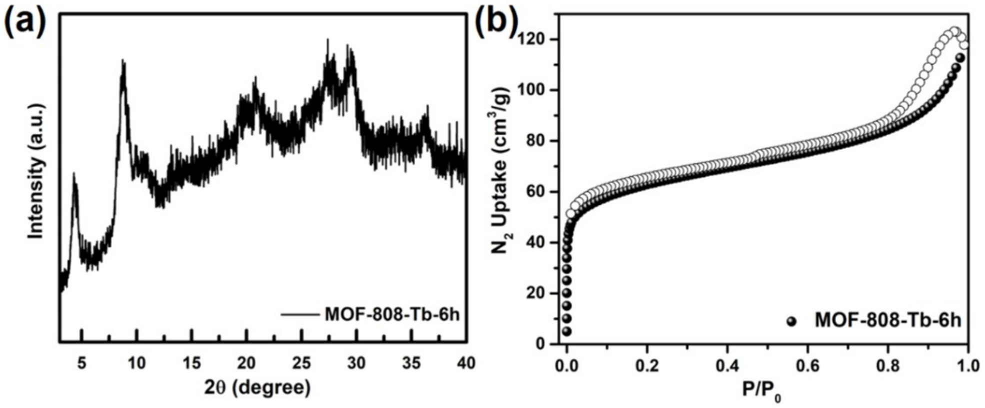

Fig. S9. (a) The PXRD pattern and (b) 77 K N_2 sorption isotherm of as-synthesized MOF-808-Tb-6h. Closed symbol, adsorption; open symbol, desorption.

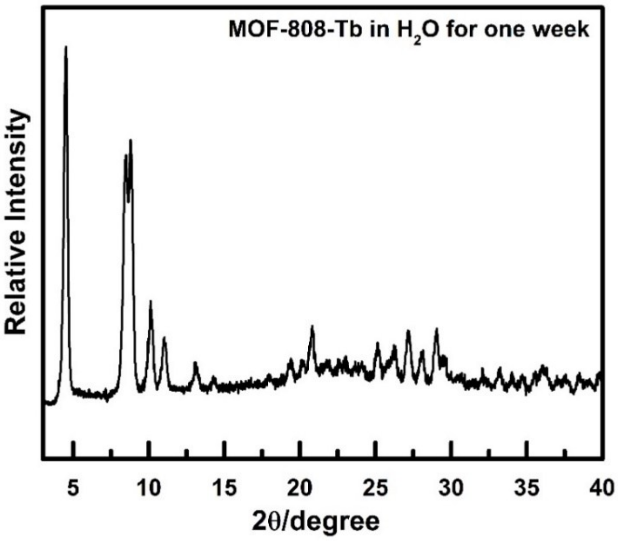

Fig. S10. The PXRD pattern of as-synthesized MOF-808-Tb after treatment with water for one week.

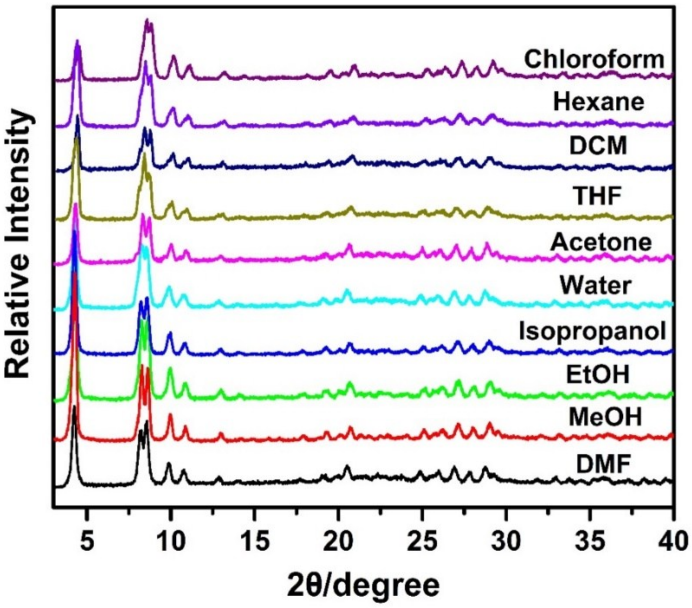

Fig. S11. The PXRD pattern of as-synthesized MOF-808-Tb immersing in various solvents for 24 h.

Luminescent Tests of as-synthesized samples

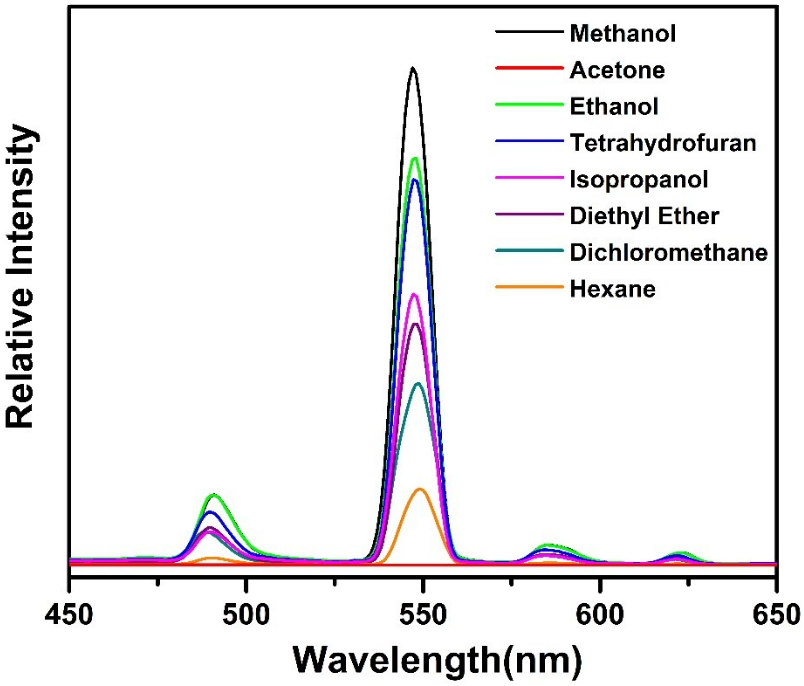

Fig. S12. Fluorescence emission spectra of MOF-808-Tb suspended in various organic solvents.

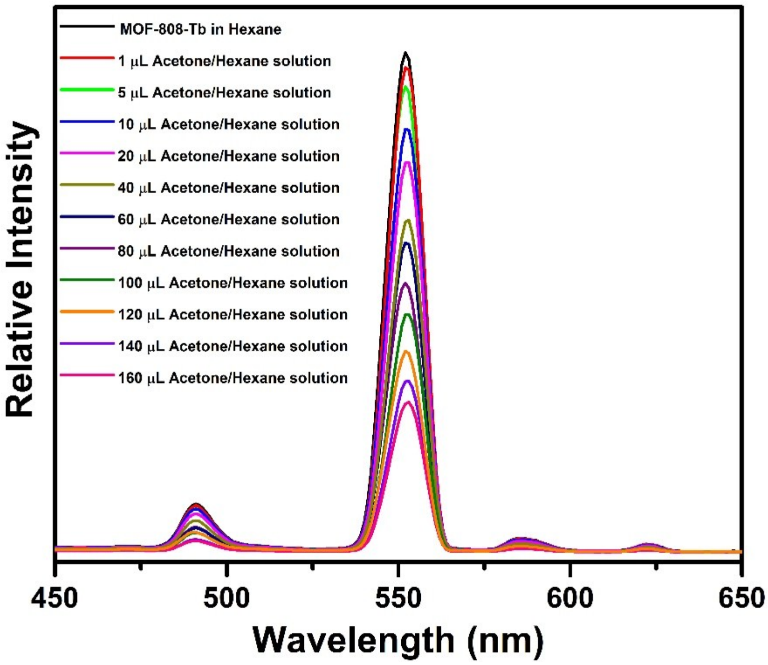

Fig. S13. Fluorescence emission spectra of MOF-808-Tb versus acetone/hexane mixture ($V_{acetone}/V_{hexane}$ = 1:1000) addition in hexane suspension (1 μL is around 0.6 ppb in hexane solution).

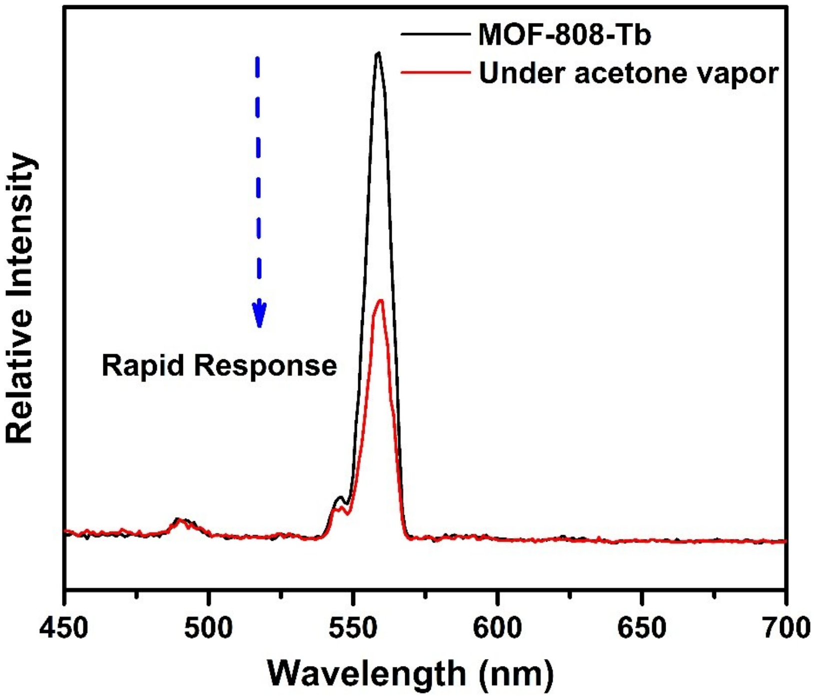

Fig. S14. Solid-based fluorescence emission spectra of MOF-808-Tb before and after acetone vapor addition (below 500 ppm).

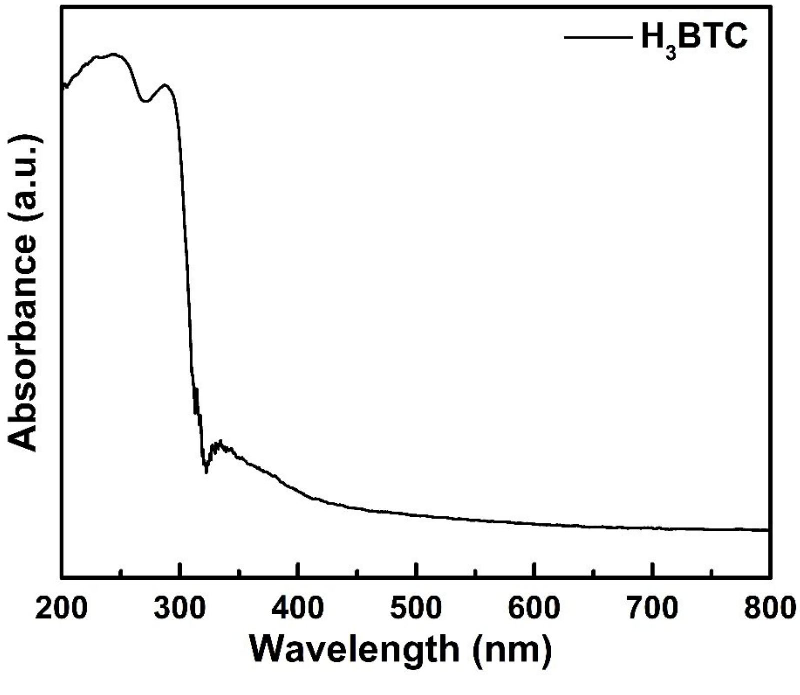

Fig. S15. Solid based UV-Vis absorption spectra of H_3BTC ligands.

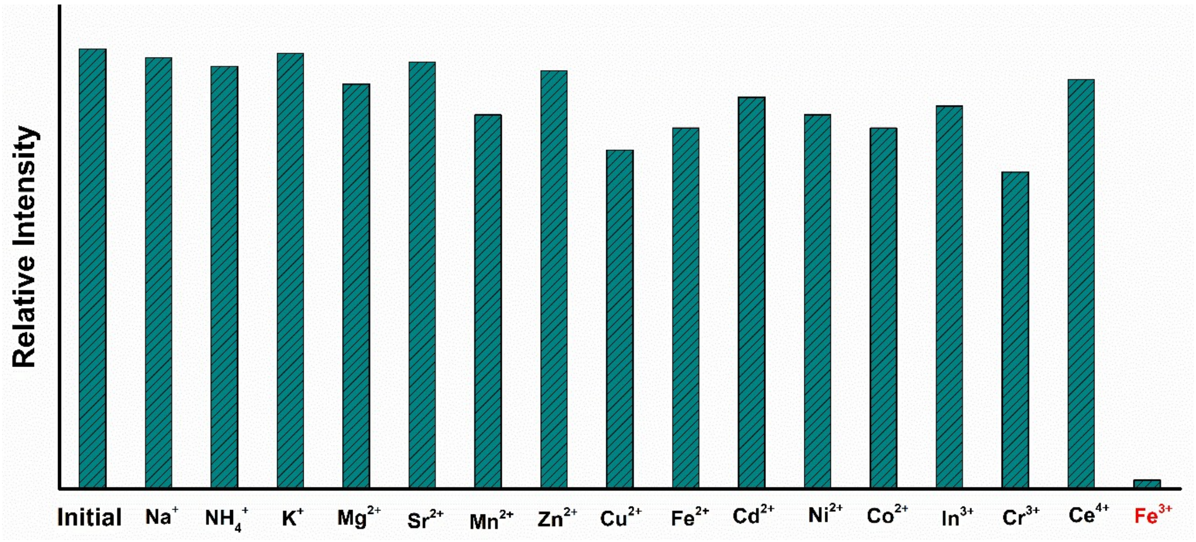

Fig. S16. Relative intensity of fluorescence emission of MOF-808-Tb after adding 200 μL of different metal ion aqueous solutions (10^{-2} M, c = 0.2 mg/mL).

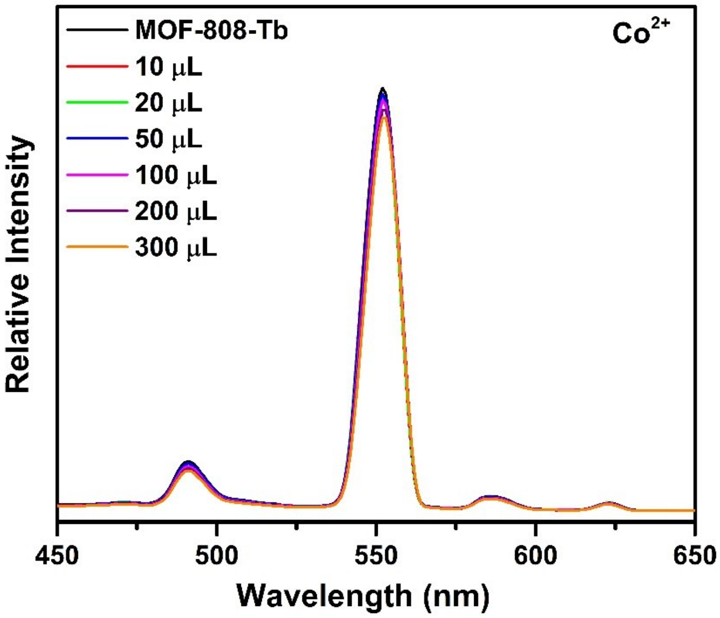

Fig. S17. Fluorescence emission spectra of MOF-808-Tb versus Co^{2+} aqueous solution (10^{-2} M) addition in water suspension.

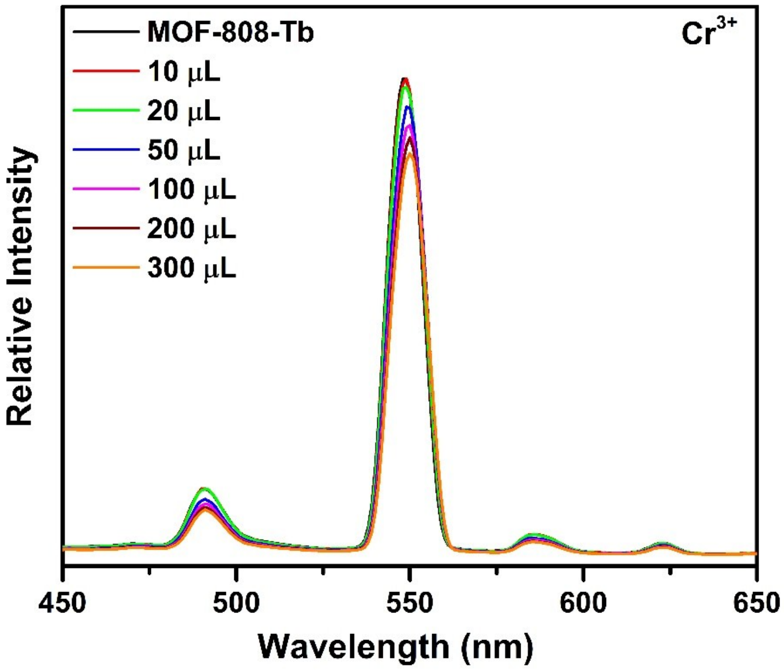

Fig. S18. Fluorescence emission spectra of MOF-808-Tb versus Cr^{3+} aqueous solution (10^{-2} M) addition in water suspension.

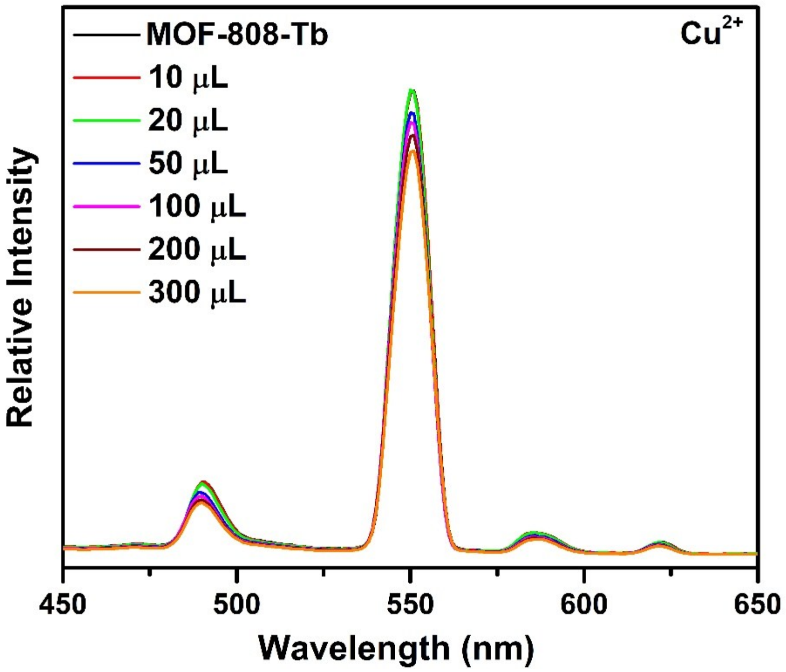

Fig. S19. Fluorescence emission spectra of MOF-808-Tb versus Cu^{2+} aqueous solution (10^{-2} M) addition in water suspension.

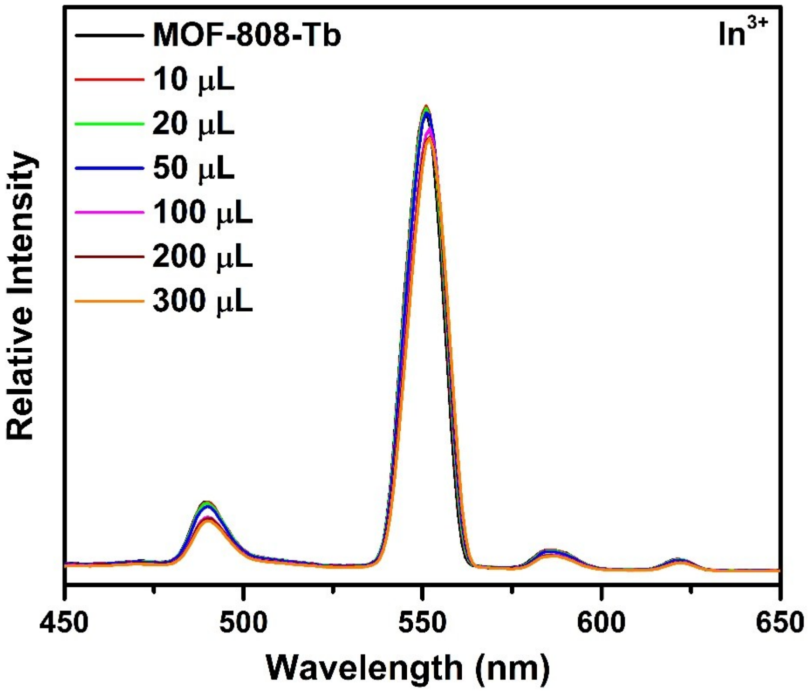

Fig. S20. Fluorescence emission spectra of MOF-808-Tb versus In^{3+} aqueous solution (10^{-2} M) addition in water suspension.

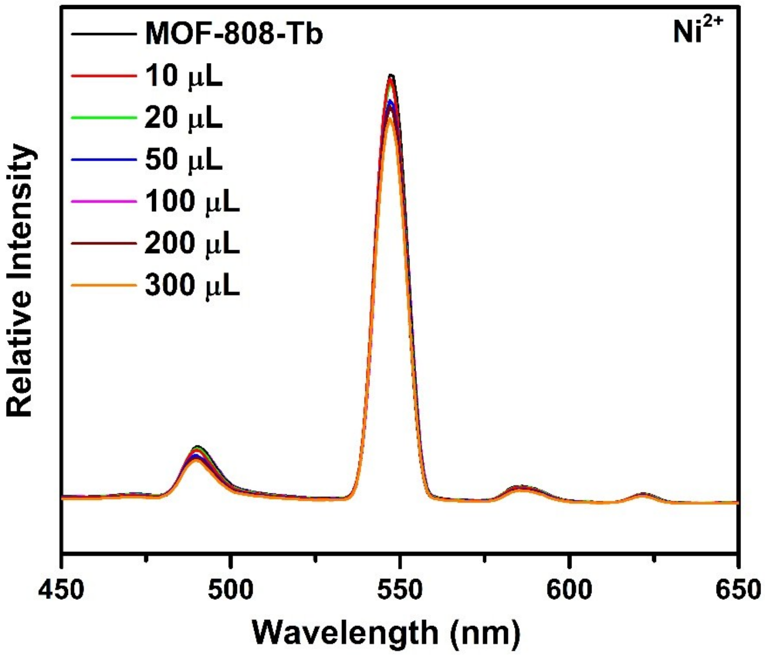

Fig. S21. Fluorescence emission spectra of MOF-808-Tb versus Ni^{2+} aqueous solution (10^{-2} M) addition in water suspension.

Mechanism Study

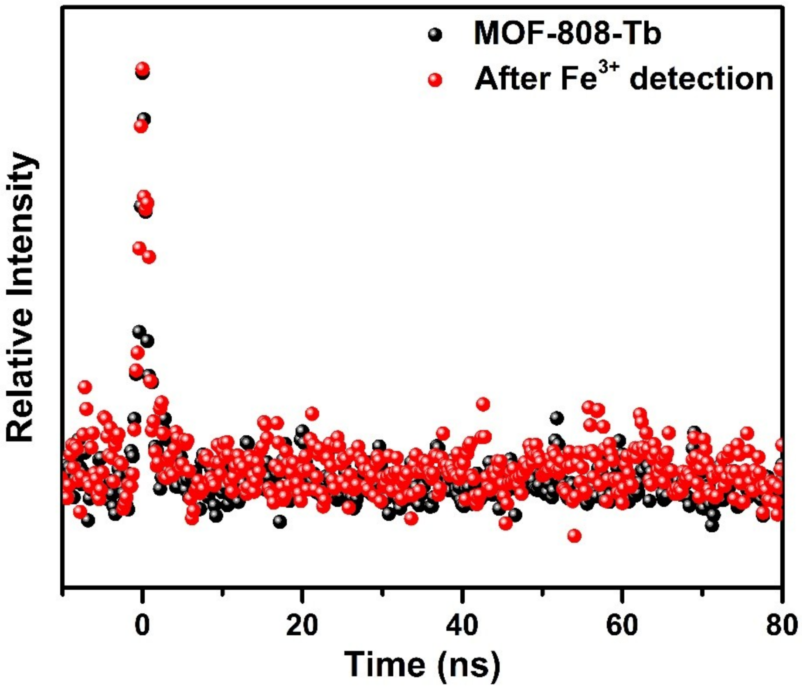

Fig. S22. Emission decay trace of MOF-808-Tb before and after the sensing experiments.

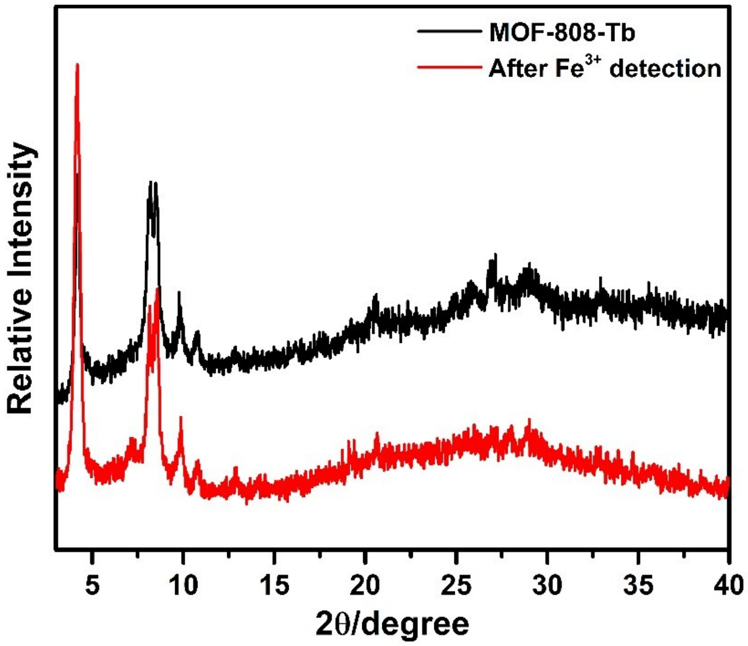

Fig. S23. The PXRD patterns of MOF-808-Tb before and after Fe^{3+} detection in aqueous solution.

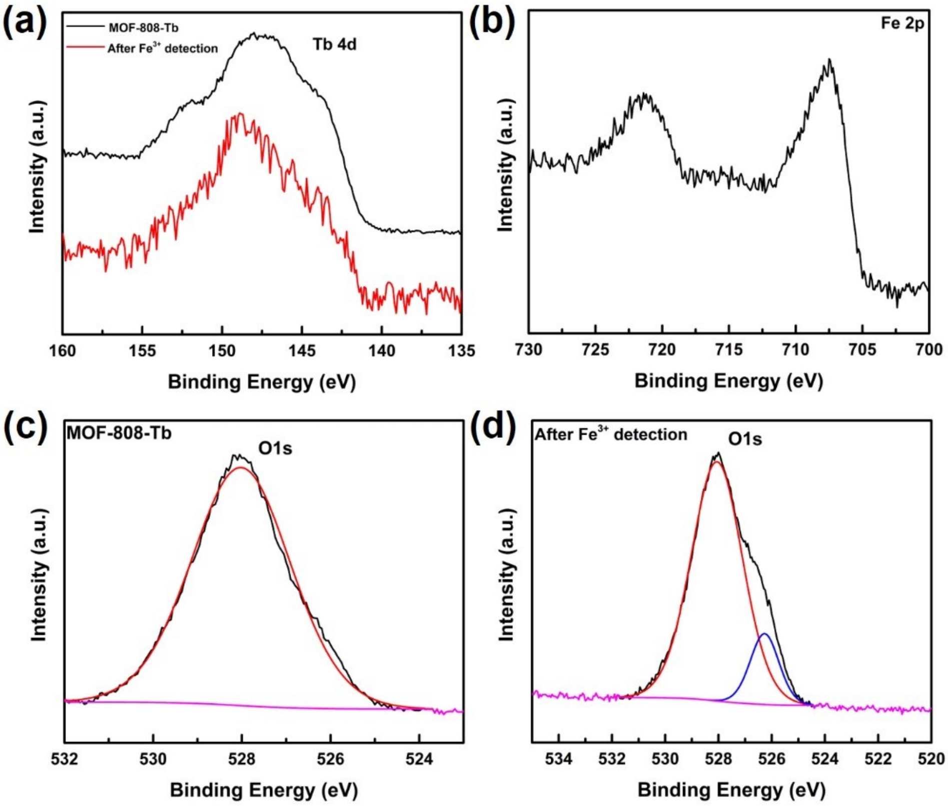

Fig. S24. Detail XPS spectra of MOF-808-Tb before and after sensing experiment: (a) Tb 4d region, (b) Fe 2p region, (c) and (d) O 1s region, respectively.

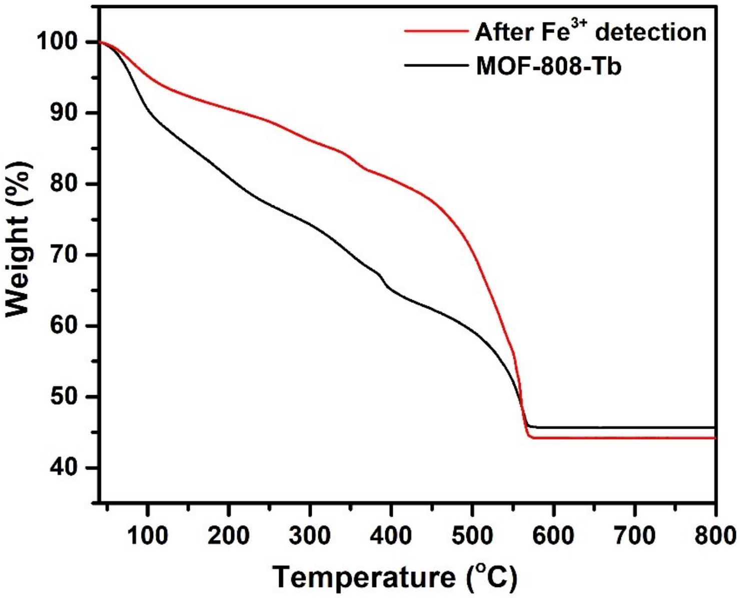

Fig. S25. The TGA curves of MOF-808-Tb before and after sensing experiment.

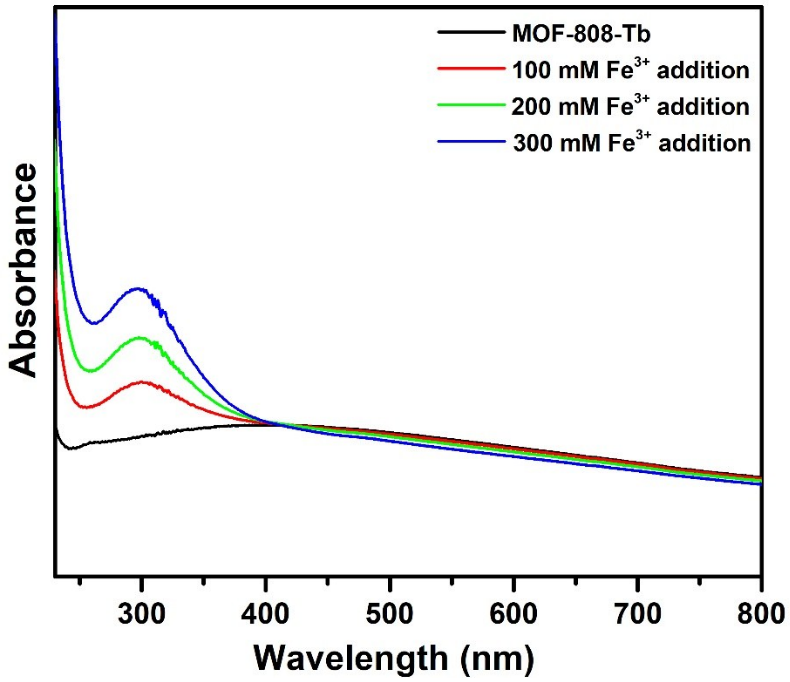

Fig. S26. UV absorption spectra of MOF-808-Tb versus Fe^{3+} aqueous solution addition in water suspension (c = 0.2 mg/mL).

Supplementary Tables

Table S1. Detailed contents of Zr, Tb, and Fe elements in the materials.

	Zr Content (%)	Tb Content (%)	Fe Content (%)
	ICP cal.	**ICP cal.**	**ICP cal.**
MOF-808	**43.12**	**NA**	**NA**
MOF-808-Tb	**40.73**	**6.88**	**NA**
After Fe^{3+} detection	**41.84**	**4.23**	**1.62**
MOF-808-Tb-0.02MFe^{3+}	**40.79**	**1.16**	**2.38**
MOF-808-Tb-0.05MFe^{3+}	**38.92**	**0.13**	**4.16**

Table S2. Comparison of detection capacities of MOF-808-Tb towards Fe^{3+} ion in water with other materials.

Materials	K_{sv} (M^{-1})	Reference
$Ln(cpty)_3$	4.10×10^3	*ACS Appl. Mater. Interfaces*, 2013, **5**, 1078-1083
Benzimidazole-based sensor	8.51×10^4	*Dyes Pigments*, 2013, **97**, 475-480
Eu^{3+}@MIL-53-COOH (Al)	5.12×10^3	*J. Mater. Chem. A*, 2014, **2**, 13691-13697
Tb-DSOA	3.54×10^3	*J. Mater. Chem. A*, 2015, **3**, 641-647
$Gd_6(L)_3(HL)_2(H_2O)_{10}$	7.89×10^2	*RSC Adv.*, 2016, **6**, 61725-61731
Eu-BPDA	1.25×10^4	*New J. Chem.*, 2016, **40**, 8600-8606
1-Eu	3.27×10^5	*Chem. Eur. J.*, 2016, **22**, 16230-16235
BUT-14	2.17×10^3	*ACS Appl. Mater. Interfaces*, 2017, **9**, 10286-10295
Cd-MDIP	4.13×10^5	*Dalton Trans.*, 2018, **47**, 9267-9273
FJI-C8	8.25×10^4	*Dalton Trans.*, 2018, **47**, 3452–3458
$Tb_4(L)_2(HCOO)(OH)_3O(DMF)_2(H_2O)_4$	1.66×10^5	*ACS Appl. Mater. Interfaces*, 2018, **10**, 23976-23986
$[Zn_3(L)_2(bipy)(OH)_2]\cdot3H_2O$	2.30×10^4	*Sensors and Actuators B*, 2018, **257**, 207-213
MOF-808-Tb	3.12×10^5	This work